AKADÉMIAI KIADÓ

UNIVERSITY of DEBRECEN

International Review of Applied Sciences and Engineering

14 (2023) 1, 45–57

DOI:
10.1556/1848.2021.00413

ORIGINAL RESEARCH PAPER

*Corresponding author.
E-mail: sahiny@erciyes.edu.tr

AKJournals

Performance analysis of multi rotor drone systems with changeable rotors

Şahin Yildirim[1]* and Muhammed İşci[2]

[1] Department of Mechatronics Engineering, Faculty of Engineering, Erciyes University, Kayseri, Turkey

[2] Department of Mechatronics, Technical Sciences Vocational School, Kayseri University, Kayseri, Turkey

Received: November 10, 2021 • Accepted: December 13, 2021
Published online: October 6, 2022

ABSTRACT

Due to some failure during the flying of drone systems, it is necessary to design and analyse compact and changeble muti rotor drone systems by using softwares. Multi-engine aircrafts are the mechatronic systems consisting of body frame, electronic control systems, rotors and blades. In the simulations realized in this work special focus has been given to the body frame due to the presence of mechanical and electronic components inside. Analysis of different vibration and force effects occurring on the whole system during the flight with high accuracy is vital for the design process of multi-engine aircrafts. In this work, a novel design procedure has been applied for the multi-engine aircraft structures including 4, 6, 8, 10 and 12 rotors and then the vibration and force effects occurring during the flight have been analyzed. As a result of detailed modal analysis carried out for different vibration frequencies, it has been observed that the vibration frequencies occurring during the flight vary between 7 and 10 Hz. Moreover, from the results obtained, it has been observed that the vibration frequency decreases while the number of rotors increased. As a result of these decreases in the vibration frequency, it has also been observed that the deformations in the body frame increased.

KEYWORDS

multi rotor, drone system, ANSYS, vibration, force

1. INTRODUCTION

In the last decades, the design of multi-engine aircrafts has become a very important purpose of research due to their constantly increasing usage areas and simple design processes. Drones are one of the most widely used multi-engine aircraft types especially in different areas such as military, security, agriculture, cartography and advertising. The drones usually consist of 4, 6 or 8 rotors and the number of rotors used directly affects both their capability of flight and load capacity. The movement produced by a drone can be controlled both manually or autonomously by changing the angular speeds of rotors. While the deflection movements usually appear as a result of the angular speed differences between the motors rotating in opposite directions, the movements of inclination and rolling are caused by the angular velocity differences between the mutually positioned rotors. While inclination and rolling movements can be relatable to translational movements for horizontal (xy) plane, for z plane they are related to the total thrust generated by the rotors.

The own mass of a drone and the total mass which can be carried by it have to be determined in the first step of the design process. In order to reduce the mass and increase the maneuverability during the flight, lightweight composite materials have to be preferred in the design process. On the other hand, the operation, steering and landing of drones are generally controlled by using control cards each communicating with 2.4 MHz frequency radio waves. A drone also consists of the following hardware: electronic speed control device (ESC), motor driver circuit, flight controller (FC), video transmitter (VTX), antenna, receiver, sensors, accelerometer, and camera. In addition to the aforementioned basic hardware, some advanced drone structures may also include Global Positioning System (GPS) modules.

In literature, there are several works analyzing the design process of drones. In [1–4], detailed analysis have been realized for the number of rotors, arm length and carrying capacity parameters by taking into account the operating conditions and areas of use. Kršák and his friends have analyzed the accuracy of the digital elevation model (DEM) which was obtained by using 4-rotor low-cost UAV photogrammetry [5]. The effects of imaging angle on 3D cliff face reconstruction in a 4-rotor UAV have been analyzed by Jaud et al. in [6]. In another work dealing with the usage of a 4-rotor Unmanned Aerial Vehicle (UAV) technology, the identification of ruts and potholes on the road surface has been carried out [7]. In [8], a UAV with 6 rotors has been designed by Verbeke and his friends to provide safe and efficient flight, especially in narrow corridors. In [9], the authors have tried to increase the efficiency by using different motor types in a multi-rotor structure with 8 rotors in total, 4 short and 4 long arms. The design of a universal and independent multi-rotor system has been realized by Niemiec and his friends in [10]. In the system designed, a reconfigurable multicopter concept has been presented between a quadcopter, hexacopter, octocopter and decacopter. Finally, in [11], analyses have been carried out on multi-rotor UAV systems with easily and quickly rechangible configuration.

In this work, detailed stress analyses have been realized for the drones designed with lightweight composite materials. As a result of the analyses carried out separately for different drone structures containing 4, 6, 8, 10 and 12 rotors, it can be concluded that the operating frequency value decreases with the increase in the number of rotors on the same body frame. It has also been observed that the vibration effects generally occur in the motor holder and arm regions. Furthermore, it was seen that the total deformation occurring in the regions exposed to vibration increases with the increase in the number of rotors. Thus, traditional design processes have been proposed for the drone structures with different number of rotors.

2. MATERIALS AND METHODS

2.1. Design of multi rotors

In this work, the drone structures with 4, 6, 8, 10 and 12 rotors, each of which can be controlled independently, have been analyzed. All rotor structures have been designed as to be in the same plane and the solid figures of all drones analyzed have been represented in Fig. 1.

In order to show the hardwares included in the drone structures analyzed in this work, the structure with 4 rotors has been represented in Fig. 2 as an example. Similarly, all other drone structures have been designed with the hardware represented in Fig. 2.

In order to analyze the pure effect of the rotor number used, all drones have been designed by using the same materials given in Table 1.

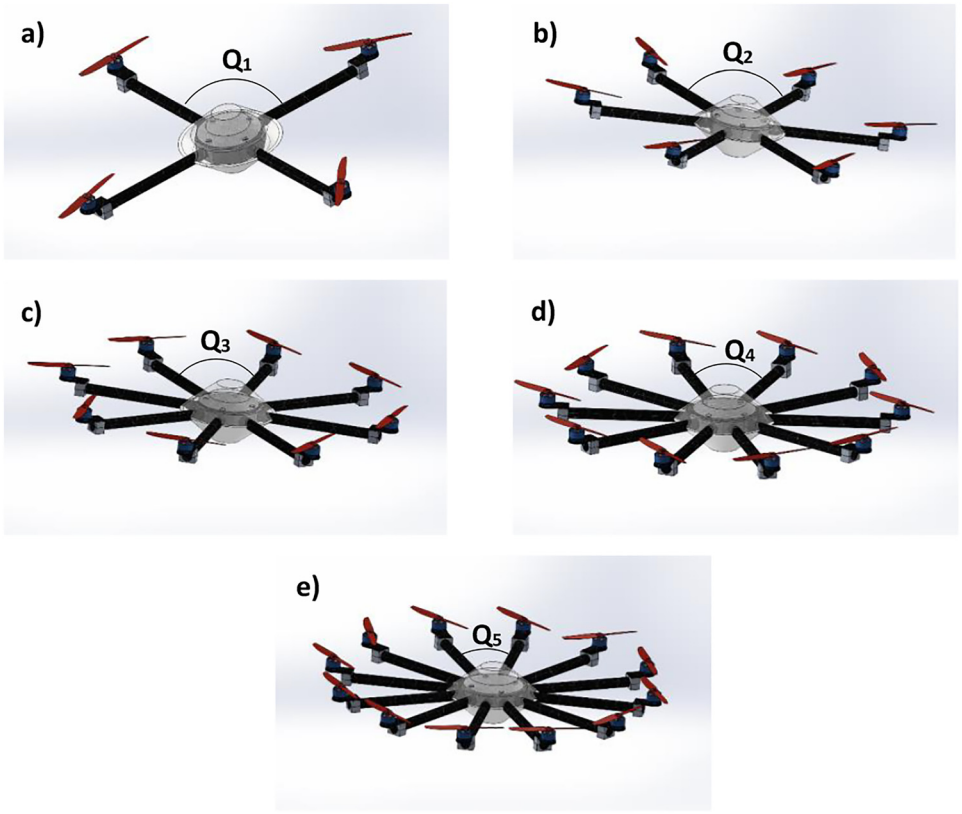

Fig. 1. Designed structures of multi drone systems a) 4 rotors, b) 6 rotors, c) 8 rotors, d) 10 rotors, e) 12 rotors

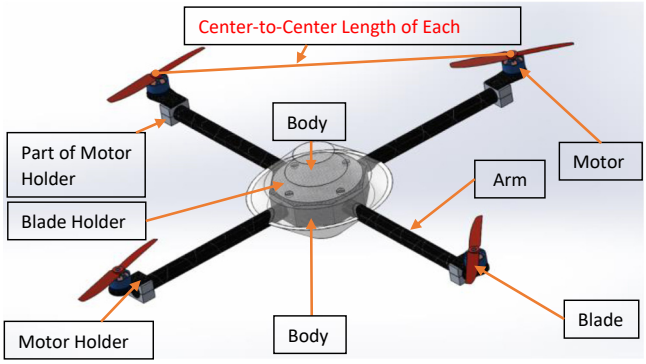

Fig. 2. Main description of the proposed drone structure with 4 rotors

Table 1. Material types of each hardware used

Hardware	Material Type
Arm of Drone	Polyethylene
Body of Drone	Polyethylene
Blade Holder	Polyethylene
Motor Holder/Part of Motor Holder	Stainless Steel

The physical properties of the drone structures designed in this work have been given below in Table 2.

2.2. Multi rotor dynamics

The coordinate plane formed around the body frame of the quadcopter structure designed in this work can be represented as in Fig. 3 [12].

The translation dynamics of a multi-rotor system in the direction of B-coordinate can be given as the following by taking into account the Newton approximation:

$$m\dot{v} + \Gamma(\omega)mv = R_q^T f_G + f_B \tag{1}$$

where, m represents the total mass; $v(t) = [v_x(t)v_y(t)v_z(t)]^T$ shows the velocity vector for the mass centre of the drone; $\dot{v}(t) = [\dot{v}_x(t)\dot{v}_y(t)\dot{v}_z(t)]^T$ represents the acceleration vector; $f_G = [0\ 0 - mg]^T$ and $f_B = [0\ 0\ U]^T$ shows the gravitational force and the total force of thrusters, repectively. Finally, the

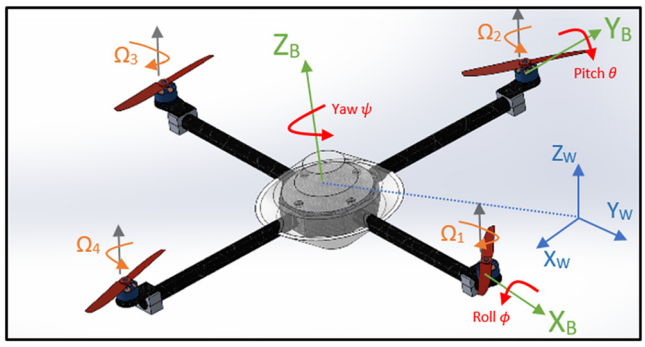

Fig. 3. The illustration of a quadcopter including body and inertia frames

cross-product matrix for the forces is represented by $\Gamma(\omega)$ and defined as the following,

$$\Gamma(\omega) = \begin{bmatrix} 0 & -\omega_z & \omega_y \\ \omega_z & 0 & -\omega_x \\ -\omega_y & \omega_x & 0 \end{bmatrix} \tag{2}$$

The Dynamics occurring through the W-coordinate, namely, $W = [X_W Y_W Z_W]^T$ can be shown as in Eq. (3),

$$\ddot{r} = \frac{1}{m}(f_G + R_q f_B) \tag{3}$$

where, $r(t) = [x(t)\ y(t)\ z(t)]^T \varepsilon R^3$ shows the position vector; since $\ddot{r} = R_q \dot{v}$.

Based on the Newton-Euler Equation, the B-coordinate rotational dynamics of a multi-rotor system can be given as in Eq. (4),

$$I\dot{\omega} + \Gamma(\omega)\mathrm{I}\omega + \tau_d = \tau \tag{4}$$

where, the symmetric inertia matrix I occurs around the mass center of the drone; the unpredicted moment disturbances are represented by $\tau_d(t) = [\tau_{d\phi}\ \tau_{d\theta}\ \tau_{d\psi}]^T$ in which the ϕ, θ and ψ parameters represent the roll, pitch and yaw, respectively. Finally, $\tau(t) = [\tau_\phi(t)\ \tau_\theta(t)\ \tau_\psi(t)]^T$ B-coordinate moment vector occurs on the onboard controller and produces the multi-rotor motion.

In the simulations realized in this work it is assumed that each motor produces both the body-aligned forces

Table 2. Physical properties of the drone structures designed

Properties	Structure				
	4-Rotors	6-Rotors	8-Rotors	10-Rotors	12-Rotors
Q_1	90°	–	–	–	–
Q_2	–	60°	–	–	–
Q_3	–	–	45°	–	–
Q_4	––	–	–	36°	–
Q_5	–	–	–	–	30°
Length of Arm	405 mm	405 mm	405 mm	405 mm	405 mm
Max. Diameter of Body	300 mm	300 mm	300 mm	300 mm	300 mm
Min. Diameter of Body	85.48 mm	85.48 mm	85.48 mm	85.48 mm	85.48 mm
Lenght of Blade	254 mm	254 mm	254 mm	254 mm	254 mm
Center-to-Center Length of Each Blade	**732.77 mm**	**512.16 mm**	**396.57 mm**	**322.28 mm**	**270.47 mm**

represented as $F_i = I\Omega_i^2$ and moments represented as $M_i = b\Omega_i^2$. In these equations, I and b are the aerodynamic force and moment constant of the rotors, respectively. The angular velocity of each motor has been constrained to an upper limit of Ω_{max} that can be determined as $|\Omega_i|<\Omega_{max}$.

The moment output occurring on an onboard control system for a plus-configuration is represented by τ and can be determined as the following,

$$\tau = \begin{bmatrix} \tau_\phi \\ \tau_\theta \\ \tau_\psi \end{bmatrix} = \begin{bmatrix} \ell I(\Omega_2^2 - \Omega_4^2) \\ \ell I(-\Omega_1^2 + \Omega_3^2) \\ b(-\Omega_1^2 + \Omega_2^2 - \Omega_3^2 + \Omega_4^2) \end{bmatrix} \quad (5)$$

where ℓ is the length from the centre of mass of the multi-rotor to the rotor. Equation (5) can be re-obtained as given following for an X-configuration in which the Blades 1 and 2 have been placed on the front side,

$$\tau = \begin{bmatrix} \tau_\phi \\ \tau_\theta \\ \tau_\psi \end{bmatrix} = \begin{bmatrix} \ell I(-\Omega_1^2 + \Omega_2^2 + \Omega_3^2 - \Omega_4^2)/\sqrt{2} \\ \ell I(-\Omega_1^2 - \Omega_2^2 + \Omega_3^2 + \Omega_4^2)/\sqrt{2} \\ b(-\Omega_1^2 + \Omega_2^2 - \Omega_3^2 + \Omega_4^2) \end{bmatrix} \quad (6)$$

For instance, for a hexacopter structure in which propellers 1 and 2 have been placed in front sides, the attitude control moment values given in Eq. (7) will be observed.

$$\tau = \begin{bmatrix} \tau_\phi \\ \tau_\theta \\ \tau_\psi \end{bmatrix} = \begin{bmatrix} \ell I\left(\frac{-\Omega_1^2}{2} + \frac{\Omega_2^2}{2} + \Omega_3^2 + \frac{\Omega_4^2}{2} - \frac{\Omega_5^2}{2} - \Omega_6^2\right) \\ \ell I(-\Omega_1^2 - \Omega_2^2 + \Omega_4^2 + \Omega_5^2)\sqrt{3}/2 \\ b(-\Omega_1^2 + \Omega_2^2 - \Omega_3^2 + \Omega_4^2 - \Omega_5^2 + \Omega_6^2) \end{bmatrix} \quad (7)$$

As mentioned above for a hexacopter, the moment values can also be modelled in a similar manner for other multi-rotor configurations.

Finally, it can be concluded that the attitude state-space equation for different types of drones can be generalized as the following by using Eq. (4) [12],

$$\dot{\omega} = I^{-1}[\tau - \Gamma(\omega)I\omega - \tau_d]. \quad (8)$$

3. RESULTS

Quasi-Static, Dynamic and Modal analyses methods are the most commonly preferred approaches in analysis of drone systems. In Quasi-Static analysis, the amplitudes of force and acceleration are accepted as too low. On the other hand, in dynamic analysis the effect of the acceleration has to be taken into consideration. These two approaches define the input–output relationship of a system for predetermined inputs. As distinct from these two approaches, in modal analysis, a detailed analysis is performed in order to determine the lower and upper limit values of the system response.

In this work, it is aimed to determine the resonance frequency at which the amplitude of the system output begins to disrupt by using the modal analysis approach.

In the design process of dynamic systems, it is vital to determine the resonance frequency with high accuracy in order to reach the maximum efficiency. After determining the resonance frequency, the working conditions of the system designed should be arranged so that the system does not fall into the resonance.

The moment values and the regions they applied in a 4-rotor drone system have been represented in Fig. 5 below.

Mode to mode resonance frequency variations obtained for all drones analyzed have been given below in Fig. 4.

The total deformations emerging as a result of the moment effects have been separately given in Fig. 6 for both the whole body and its interior body. It is seen from the figure that the maximum deformations obtained for different moments and regions are occuring in the extreme regions of the motor holders.

The modal analysis results (Mode 1) obtained for a 4-rotor drone structure with an operating frequency of 7.1796 Hz are shown in Fig. 7(a). In Mode 1 structure, it is seen that deformations especially occur in the two blades and their motor holder parts.

The results obtained for a 7.1836 Hz 4-rotor drone structure (Mode 2) and given in Fig. 7(b) show that for Mode 2 structure especially the two blades and their motor holder parts are exposed to deformations.

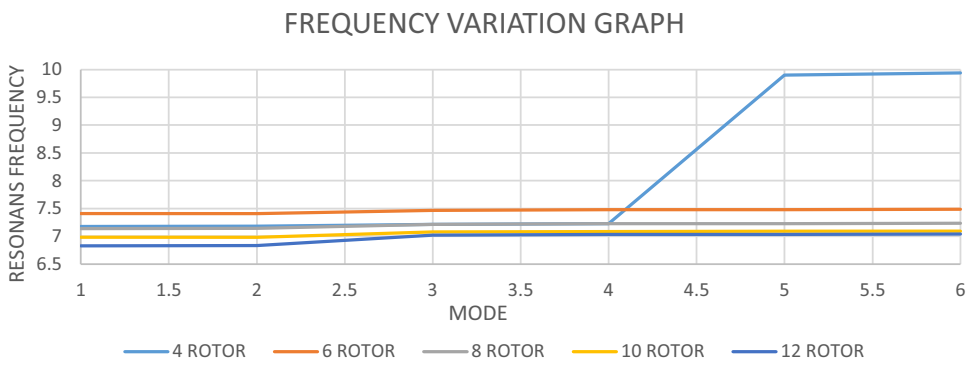

Fig. 4. Mode to mode resonance frequency variations obtained for drones

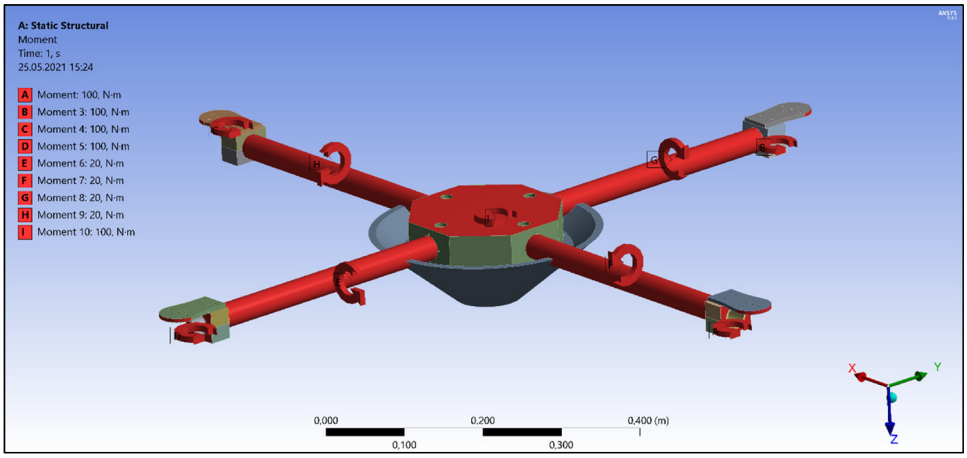

Fig. 5. The moment values and the regions they applied in the simulations realized for a 4-rotor drone system

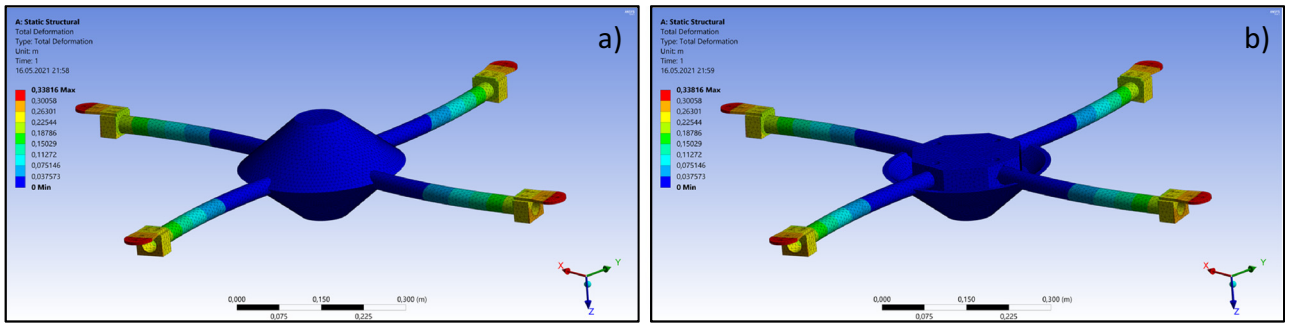

Fig. 6. Deformations occurring due to the moment affects in the 4-rotor drone system; a) Main body, b) Interior body

As seen from the results in Fig. 7(c), which were obtained for a drone structure including 4-rotors with 7.2172 Hz frequency (Mode 3), it is seen that the total deformation occurs especially in the four blades and relevant motor holder parts. It can also be concluded for Mode 3 structure that the blades and their motor holders located opposite to each other will show almost the same behavior.

In Fig. 7(d), modal analysis results emerged for a 4-rotor drone structure with a 7.225 Hz operating frequency (Mode 4) have been represented. It is seen that the total deformation may occur especially in the four blades and their motor holder parts. It can also be predicted that opposite blades and motor holders may show similar features.

In Mode 5 structure consisting of 4 rotors operating with the frequency of 9.8999 Hz, it can be expressed that the total deformation may occur especially in the four blades and their relevant motor holder parts. Moreover, similar to the other structures mentioned above opposite blades and motor holders will show behaviours similar to each other.

Finally, the results represented in Fig. 7(f) for 9.939 Hz 4-rotor structure (Mode 6) proves that only the two blades and their motor holder parts are affected by the deformations emerging due to the moments applied.

The drone structure including 6 rotors has been analyzed for the moment values and regions represented in Fig. 8.

The total deformations occurring on both the main body and the interior body as a result of the moment affects have been represented in Fig. 9. As seen from the figure, the maximum deformations are frequently emerging around the extreme regions of the motor holders.

The total deformations obtained for a 7.4069 Hz 6-rotor drone structure (Mode 1) are given in Fig. 10(a). The modal analysis results of Mode 1 shows that the total deformation especially occurs at the four blades and their relevant motor holder parts.

In Mode 2 structure consisting of 6 rotors operating with the frequency of 7.4117 Hz, as a result of the simulations it is seen that all the blades and their relevant motor holder parts are affected by the deformations due to the moment affects.

The modal analysis results given in Fig. 10(c) for 7.465 Hz 6-rotor drone structure (Mode 3) represents that five blades and their motor holder parts produce similar deformation results as obtained in Mode 2.

The modal analysis results given in Fig. 10(d) for Mode 4 represents that the 7.4822 Hz 6-rotor drone structure produces similar deformation results as obtained in Mode 2.

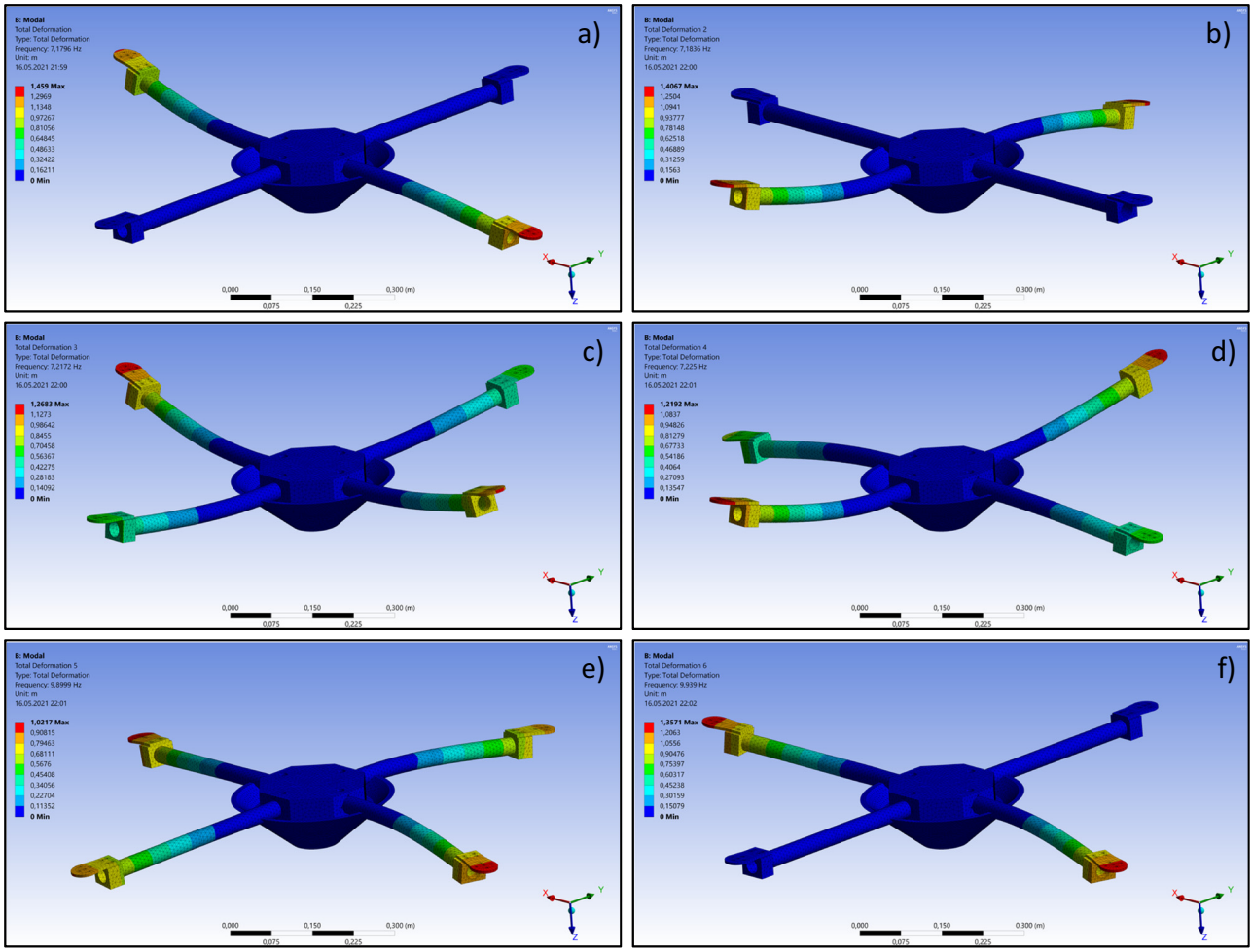

Fig. 7. Modal analysis results obtained for the 4-rotor drone system a) Mode 1, b) Mode 2, c) Mode 3, d) Mode 4, e) Mode 5, f) Mode 6

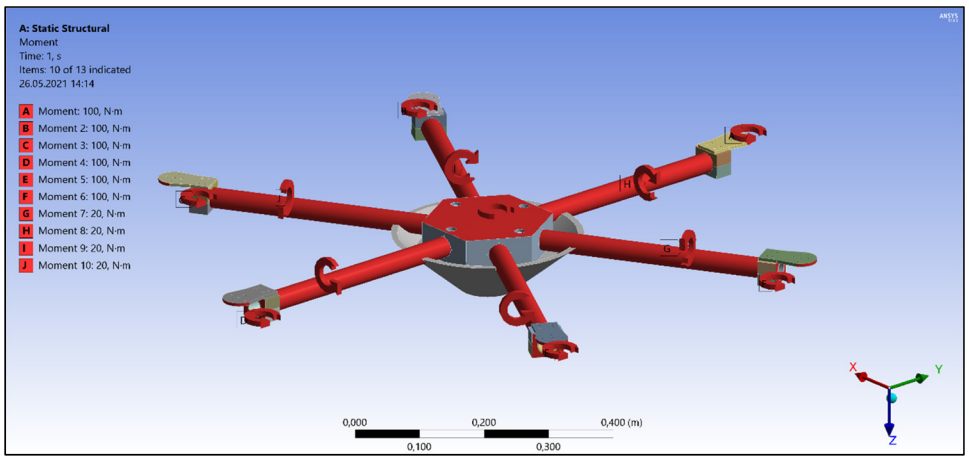

Fig. 8. The moment values and the regions they applied in the simulations realized for a 6-rotor drone system

As seen from the Mode 5 results given in Fig. 10(e) for the drone structure including 6 rotors operating with 7.4829 Hz deformations emerge in all the blades and their relevant motor holder parts.

Finally, the results presented in Fig. 10(f) for 7.4896 Hz 6-rotor structure (Mode 6) proves that the deformations occurring affects the blades and their motor holder parts as in the previous mode structures.

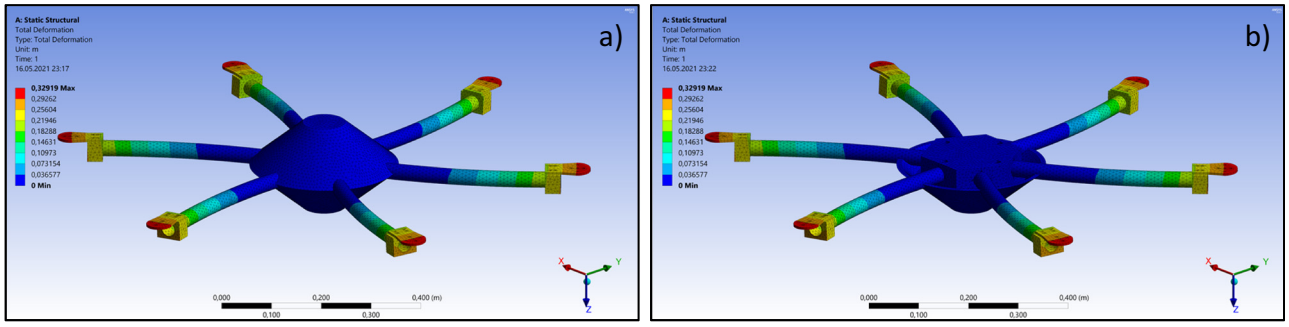

Fig. 9. Deformations occurring due to the moment affects in the 6-rotor drone system; a) Main body, b) Interior body

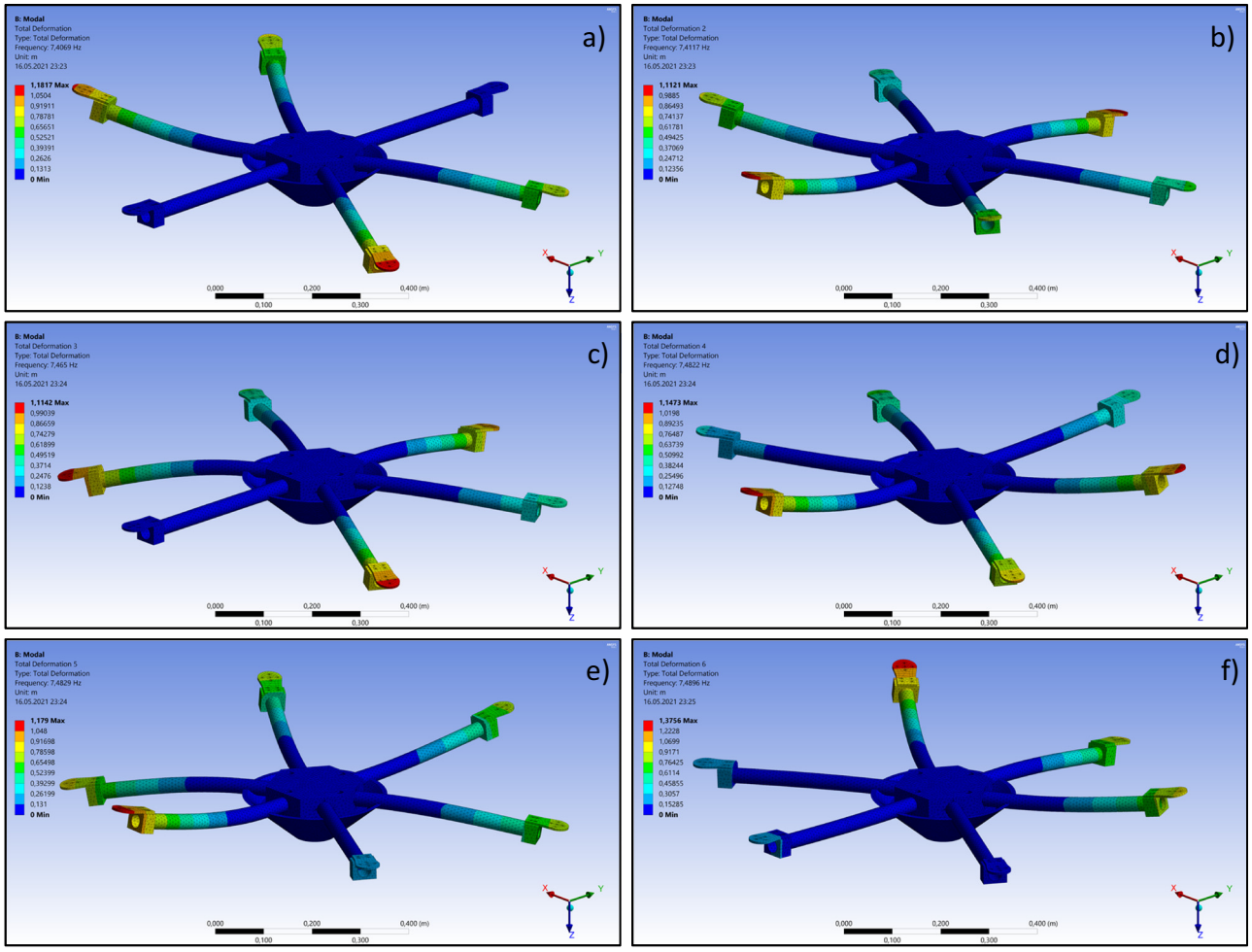

Fig. 10. Modal analysis results obtained for the 6-rotor drone system a) Mode 1, b) Mode 2, c) Mode 3, d) Mode 4, e) Mode 5, f) Mode 6

The moment values and regions applied for the 8-rotor drone structure are given in Fig. 11 below.

In Fig. 12(a), deformations occurring due to the moment effects have been shown separately for each blade and relevent motor holder parts. When the figures given for the main and the interior bodies have been analyzed, it can be concluded that the maximum deformations emerge especially in the extreme regions of the motor holders.

The modal analysis results (Mode 1) obtained for a 8-rotor drone structure with an operating frequency of 7.1405 Hz are shown in Fig. 13(a). It is observed from the figure that the deformations occur especially in the 6 blades and their relevant motor holder parts. It is also seen that the

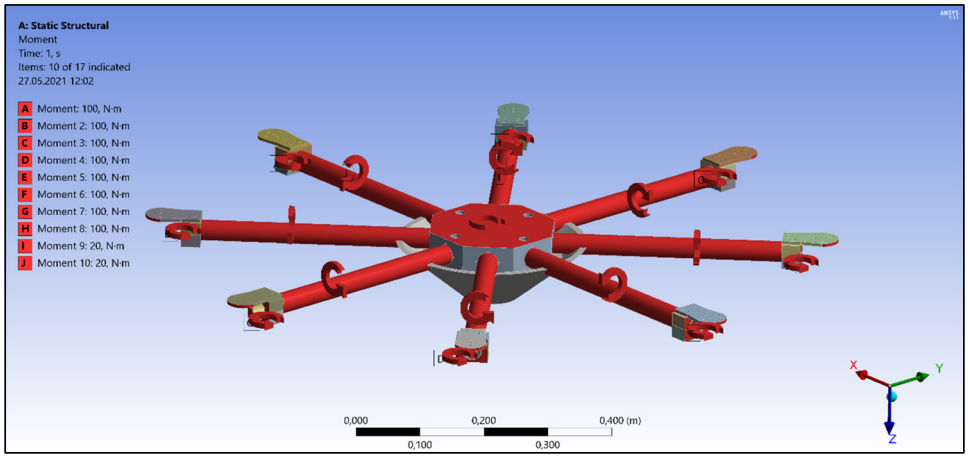

Fig. 11. The moment values and the regions they applied in the simulations realized for a 8-rotor drone system

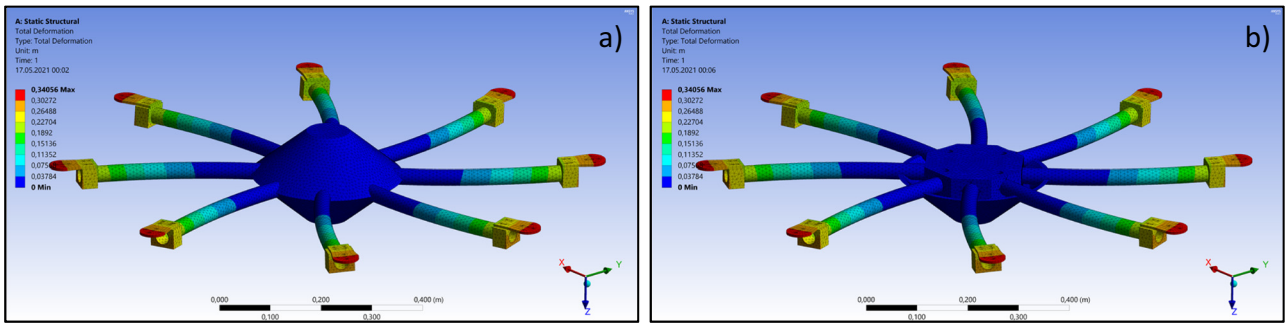

Fig. 12. Deformations occurring due to the moment affects in the 8-rotor drone system; a) Main body, b) Interior body

symmetrical blades and relevant motor holders show the same deformation properties.

In Mode 2 structure consisting of 8 rotors operating with the frequency of 7.1433 Hz, it is seen that the deformations mainly occur in all the blades and related motor holder parts.

From the Mode 3 structure consisting of 8 rotors each of which operating at the frequency of 7.2181 Hz, it is seen that all blades and their motor holder parts are significantly affected by the moment effects.

The results given in Fig. 13(d) for 7.2258 Hz 8-rotor structure (Mode 4) show that the deformations that occur due to the moment effects are especially concentrated in the 3 blades and their motor holder parts.

The Mode 5 structure which is operating at the frequency of 7.2278 Hz produces similar deformation effects as obtained in Mode 2.

Finally, the results given in Fig. 13(f) for 7.2331 Hz 8-rotor structure (Mode 6) show that the deformations that occur due to the torque effect are especially concentrated in the 4 blades and their motor holder parts.

The moment values and the regions they applied in a drone system consisting of 10 rotors have been presented in Fig. 14 below.

The deformations emerging on the whole system due to the moment effects are shown in Fig. 15(a) and (b) for the main body and interior body, respectively. It has been determined that the maximum deformations obtained occur especially in the motor holder bodies and related extreme regions.

For the Mode 1 structure which includes 10-rotors with 6.9822 Hz frequency, similar deformation effects with the previous drone types have been observed. All the blades and the relevant motor holders are being affected by the deformation. Moreover, it can be concluded that symmetrical blades and motor holders are also exposed to similar effects.

The results which were obtained for a 6.9849 Hz 10-rotor drone structure (Mode 2) and given in Fig. 16(b) show that especially 8 of the 10 blades and their motor holder parts are exposed to deformations.

As seen from the Mode 3 results given in Fig. 16(c) for the drone structure including 10 rotors, each of which operate at 7.4829 Hz frequency, deformations emerge in all the blades and their relevant motor holder parts. It can also be concluded that the blades and their motor holders located opposite to each other will show almost the same behavior.

The results given in Fig. 16(d) for the 7.089 Hz 10-rotor structure (Mode 4) show that the deformations that occur

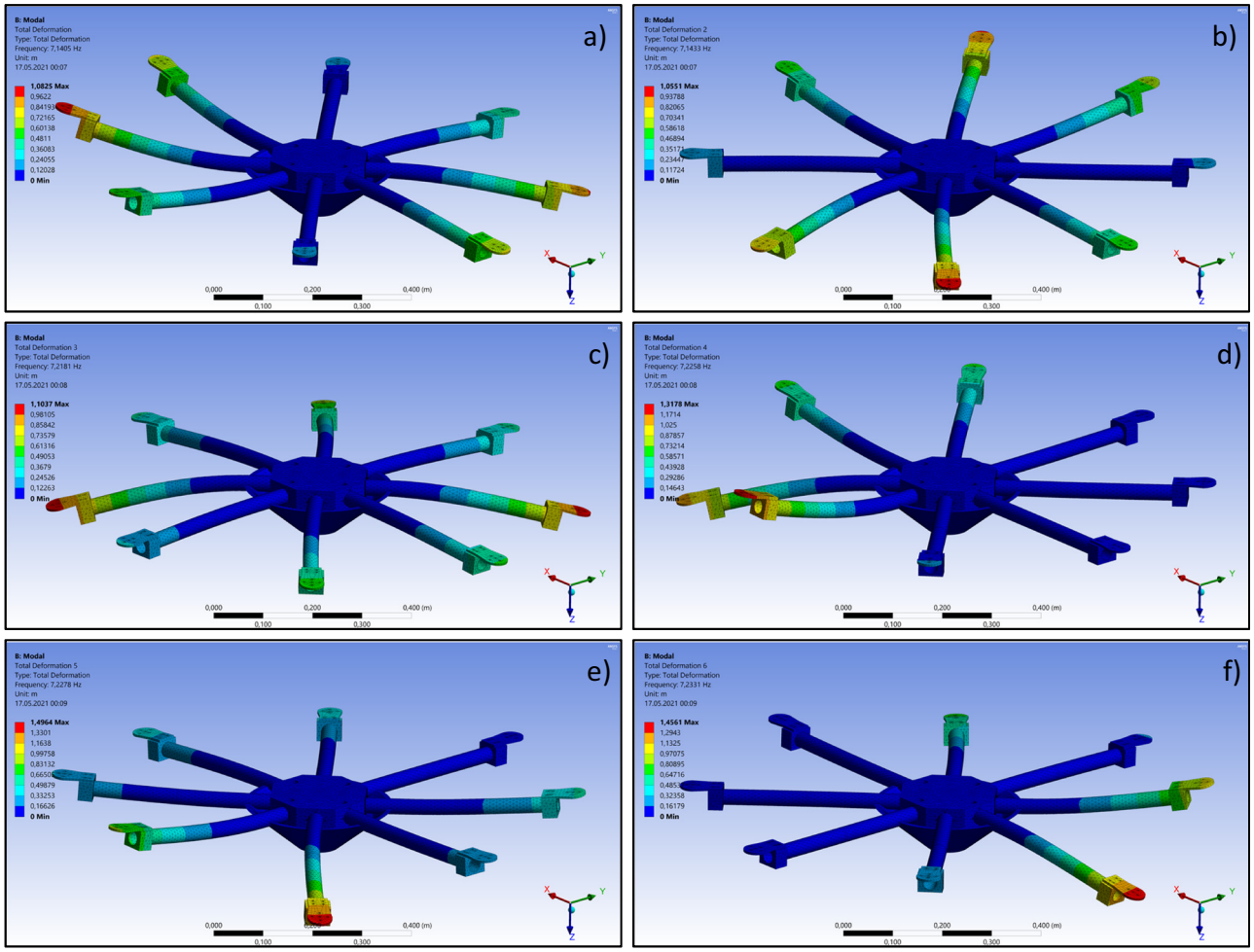

Fig. 13. Modal analysis results obtained for the 8-rotor drone system a) Mode 1, b) Mode 2, c) Mode 3, d) Mode 4, e) Mode 5, f) Mode 6

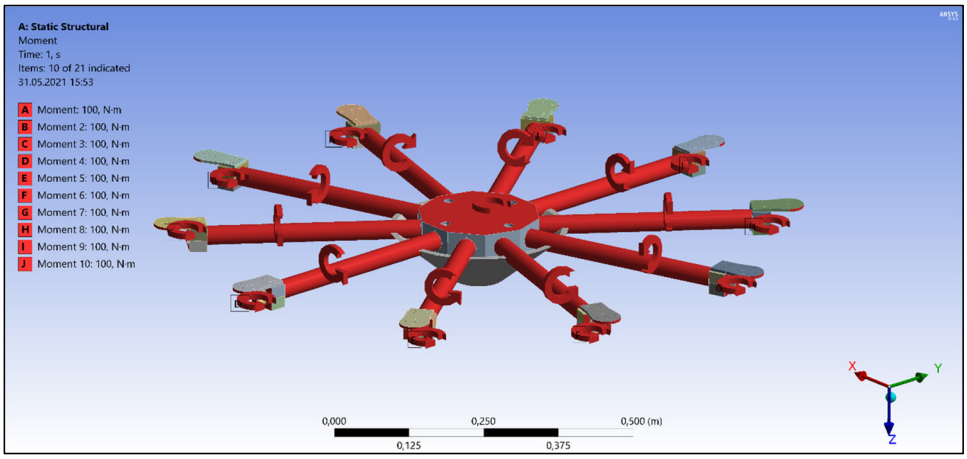

Fig. 14. The moment values and the regions they applied in the simulations realized for a 10-rotor drone system

due to the moment effects are especially concentrated in the 3 blades and their motor holder parts.

In Fig. 16(e), modal analysis results obtained for the 7.091 Hz 10-rotor drone structure (Mode 4) have been represented. As seen from the results deformation effects are occurring in 9 of the 10 blades and their motor holder parts.

Finally, in the Mode 6 structure which was analyzed under the 7.0927 Hz frequency similar results to the

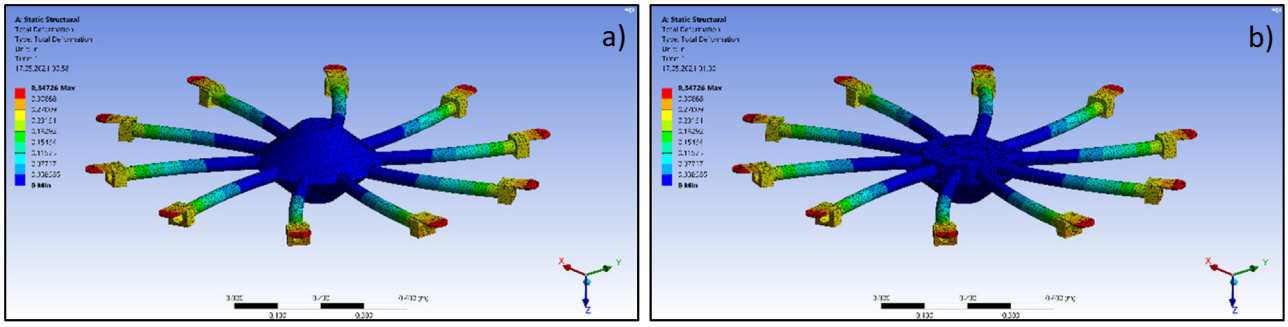

Fig. 15. Deformations occurring due to the moment affects in the 10-rotor drone system; a) Main body, b) Interior body

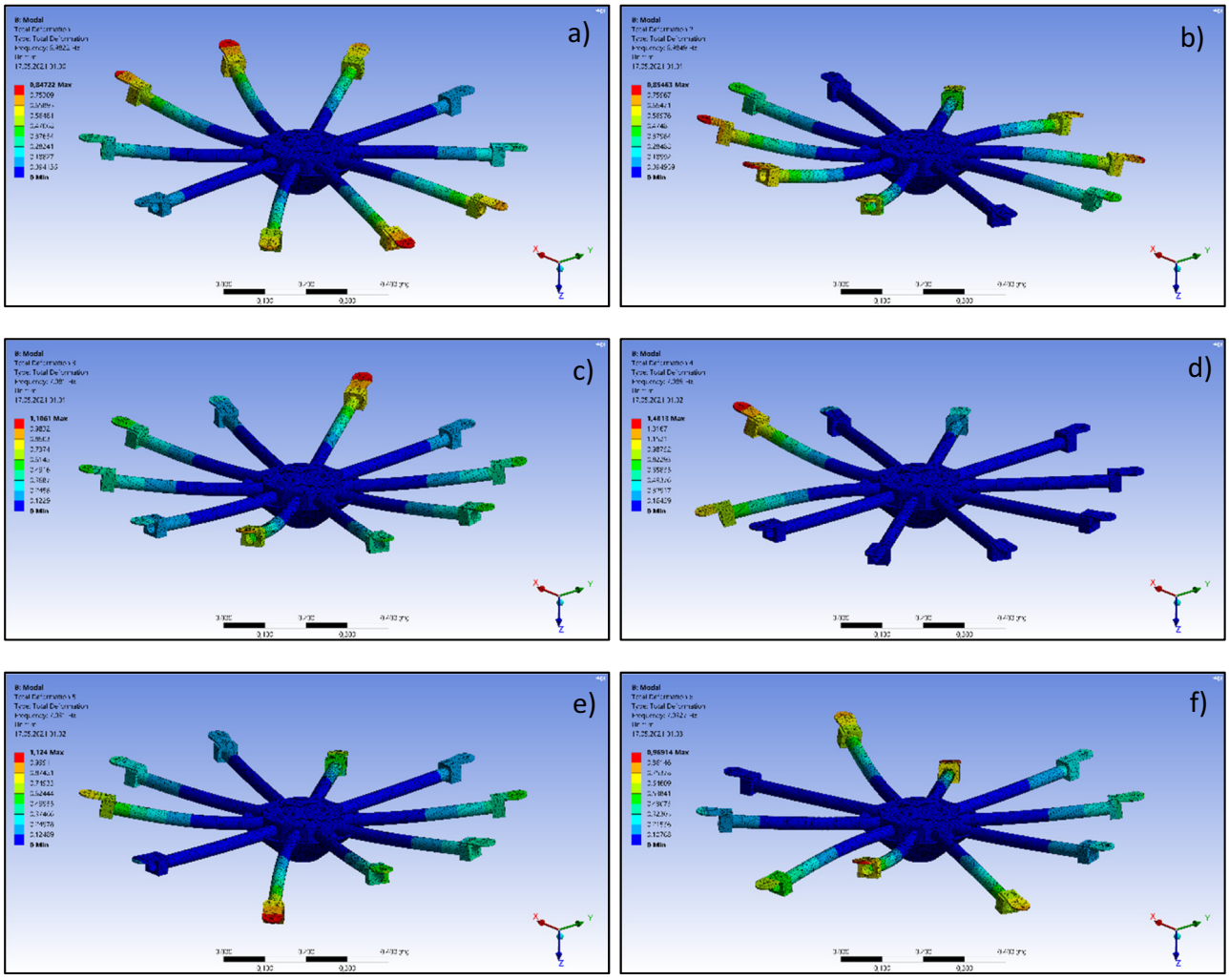

Fig. 16. Modal analysis results obtained for the 10-rotor drone system a) Mode 1, b) Mode 2, c) Mode 3, d) Mode 4, e) Mode 5, f) Mode 6

previous modes have been obtained in terms of the deformation due to the moment effect.

The last drone modal analyzed in this work is the drone structure consisting of 12 rotors as shown below (Fig. 17).

Figure 18 shows the main body and interior view deformation results obtained after applying different moments to the 12-rotor drone structure. Similar to the drone structures previously analyzed, in the 12-rotor structural deformations have been especially affecting the motor holder parts and their relevant extreme regions.

When the results obtained for the frequencies of 6.8307 Hz in Fig. 19(a) and 6.8341 Hz in Fig. 19(b) are

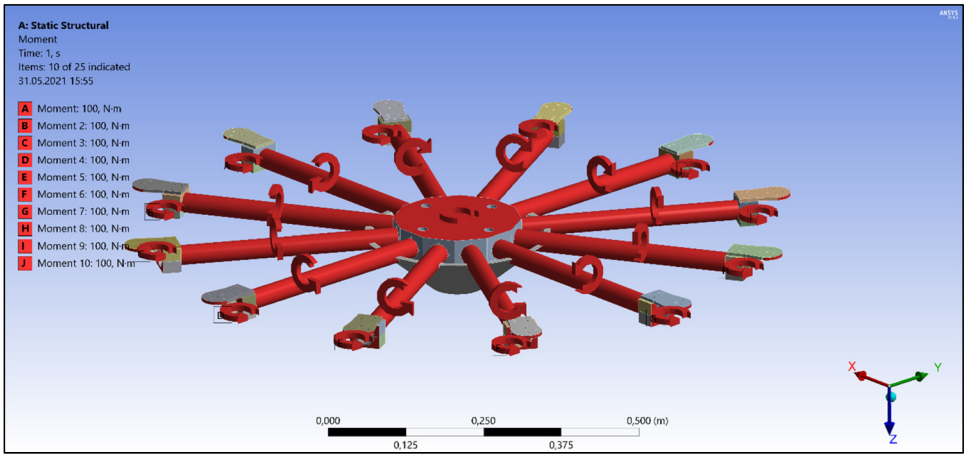

Fig. 17. The moment values and the regions they applied in the simulations realized for a 12-rotor drone system

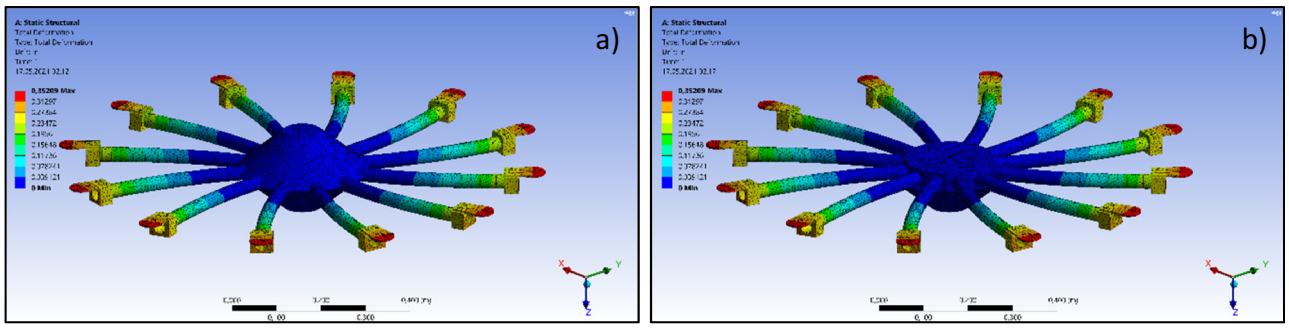

Fig. 18. Deformations occurring due to the moment affects in the 12-rotor drone system; a) Main body, b) Interior body

examined, in both Mode 1 and Mode 2 structures, it is seen that deformations appear in 10 of the 12 blades and their relevant motor holders.

In Fig. 19(c), the modal analysis result of a 12-rotor drone structure with a frequency of 7.0209 Hz (Mode 3) is given. As seen from the figure, all the blades and the relevant motor holders are being affected by the deformation. Moreover, it can be concluded that in most of the symmetrical blades and their motor holders similar moment effects occur.

In the Mode 4 structure which is operating at the frequency of 7.0343 Hz, especially 8 of the 12 blades and their relevant motor holders are exposed to the deformations emerging due to the moment effects.

The modal analysis results obtained for Mode 5 structure consisting of 12 rotors with 7.0349 Hz operating frequency represent that the lowest deformation effects are being obtained in Mode 5 structure.

Finally, the deformations occurring for 7.0396 Hz 12-rotor drone structure are given in Fig. 19(f). As seen from the figure especially 9 of the 12 blades and motor holders are being affected by the deformations.

4. DISCUSSION

In modal analysis, the possible vibration forms that may occur on the whole system can be represented by the mode states. The properties of the materials used in the design directly affect the modal parameter values. The ANSYS-based modal analyses performed in this work have been carried out under the predetermined limit conditions and with a sensitivity of 7.77e−003 m. As a result of the simulations realized for Polyethylene and Stainless Steel material based drones and 6 different modes in each drone structure, it has been observed that the maximum frequency value was obtained as 9.9 Hz (approximately 10 Hz) and the vibration frequency varies in the range of 7–10 Hz. On the other hand, it was also seen that an increase in the number of rotors causes small increases in the total deformation. The resonance occurring as a result of equalization of the frequency of external forces to the natural frequency may cause strong deformations on the system. As a result of the analyses it has been observed that as the mode value increased, the resonance frequency also increased. On the other hand, it has

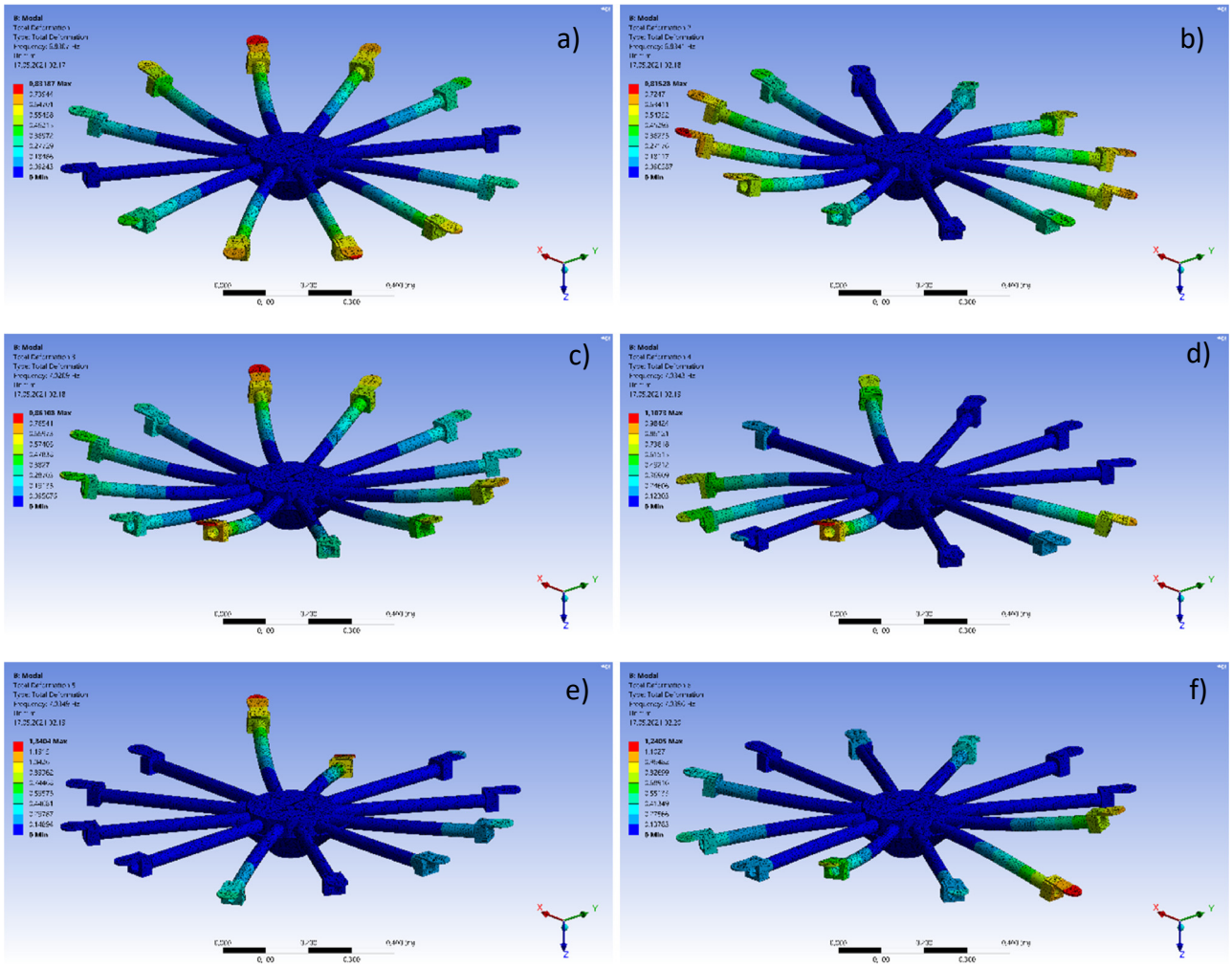

Fig. 19. Modal analysis results obtained for the 12-rotor drone system a) Mode 1, b) Mode 2, c) Mode 3, d) Mode 4, e) Mode 5, f) Mode 6

also been seen that the resonance frequency decreases with the increase in the number of rotors. In other words, when the number of rotors is increased, deformations due to low amplitude vibrations occur on the system. While the maximum total deformation value has been measured as 0.33816 m for a 4-rotor structure, it was obtained as 0.35209 m for the 12-rotor drone structure.

5. CONCLUSION

In this work, detailed design and modal analysis of drone structures with 4, 6, 8, 10 and 12 rotors have been performed. The two different moment values of 20 and 100 Nm have been applied to the regions on which the vibration and force effects were investigated. From the deformation results obtained for the drone structures with different number of rotors, it is seen that the amount of total deformation increases as the number of rotors increased. It has also been observed that the deformation regions occurred in similar coordinates to each other in all systems.

As a result of mode to mode performance comparison between the drone structures, it was seen that the blades located opposite to each other and their motor holders are affected similarly by the vibrations and force effects. Also, it can be expressed from the simulation results that negligible small vibrations will occur around the main body.

REFERENCES

[1] M. Streßer, R. Carrasco, and J. Horstmann, "Video-based estimation of surface currents using a low-cost quadcopter," *IEEE Geosci. Remote Sens. Lett.*, vol. 14, no. 11, pp. 2027–31, 2017. https://doi.org/10.1109/LGRS.2017.2749120.

[2] A. Claesson, D. Fredman, L. Svensson, M. Ringh, J. Hollenberg, P. Nordberg, M. Rosenqvist, T. Djarv, S. Österberg, J. Lennartsson, and Y. Ban, "Unmanned aerial vehicles (drones) in out-of-hospital cardiac-arrest," *Scand. J. Trauma Resusc. Emerg. Med.*, vol. 24, p. 124, 2016. https://doi.org/10.1186/s13049-016-0313-5.

[3] S. N. Ghazbi, Y. Aghli, M. Alimohammadi, and A. A. Akbari, "Quadrotors unmanned aerial vehicles: a review," *Int. J. Smart Sens. Intell. Syst.*, vol. 9, pp. 309–33, 2016. https://doi.org/10.21307/ijssis-2017-872.

[4] V. K. Gadi, A. Garg, S. Prakash, L. Wei, and S. Andriyas, "A non-intrusive image analysis technique for measurement of heterogeneity in grass species around tree vicinity in a green infrastructure," *Measurement*, vol. 114, pp. 132–43, 2018. https://doi.org/10.1016/j.measurement.2017.09.010.

[5] B. Kršák, P. Blišťan, A. Pauliková, P. Puškárová, Ľ. Kovanič, J. Palková, and V. Zelizňaková, "Use of low-cost UAV photogrammetry to analyze the accuracy of a digital elevation model in a case study," *Measurement*, vol. 91, pp. 276–87, 2016. https://doi.org/10.1016/j.measurement.2016.05.028.

[6] M. Jaud, P. Letortu, C. Théry, P. Grandjean, S. Costa, O. Maquaire, R. Davidson, and N. Le Dantec, "UAV survey of a coastal cliff face – Selection of the best imaging angle," *Measurement*, vol. 139, pp. 10–20, 2019. https://doi.org/10.1016/j.measurement.2019.02.024.

[7] A. M. Saad and K. N. Tahar, "Identification of rut and pothole by using multirotor unmanned aerial vehicle (UAV)," *Measurement*, vol. 137, pp. 647–54, 2019. https://doi.org/10.1016/j.measurement.2019.01.093.

[8] J. Verbeke, D. Hulens, H. Ramon, T. Goedeme, and J. De Schutter, "The design and construction of a high endurance hexacopter suited for narrow corridors," *Int. Conf. Unmanned Aircr. Syst. ICUAS 2014 – Conf. Proc.*, pp. 543–51, 2014. https://doi.org/10.1109/ICUAS.2014.6842296.

[9] C. E. Lin and T. Supsukbaworn, "Development of dual power multirotor system," *Int. J. Aerosp. Eng.*, vol. 2017, pp. 1–19, 2017. https://doi.org/10.1155/2017/9821401.

[10] R. Niemiec, F. Gandhi, and R. Singh, "Control and performance of a reconfigurable multicopter," *J. Aircr.*, pp. 1–12, 2018. https://doi.org/10.2514/1.C034731.

[11] S. Brischetto, A. Ciano, and C. G. Ferro, "A multipurpose modular drone with adjustable arms produced via the FDM additive manufacturing process," *Curved Layer. Struct.*, vol. 3, pp. 202–13, 2016. https://doi.org/10.1515/cls-2016-0016.

[12] O. A. Jasim and S. M. Veres, "A robust controller for multi rotor UAVs," *Aerosp. Sci. Technol.*, vol. 105, no.106010, 2020. https://doi.org/10.1016/j.ast.2020.106010.